Electronic Supplementary Material (ESI) for Journal of Materials Chemistry A.
This journal is © The Royal Society of Chemistry 2020

Electronic Supplementary Information

Iron-Regulated NiPS for Accelerated Oxygen Evolution Efficiency

Wenfeng Peng,[1a] Junkai Li,[1a] Kangqi Shen,[1b] Lirong Zheng,[c] Hu Tang,[a] Yutong Gong,[d] Junshuang Zhou,[e] Ning Chen,[f] Shijing Zhao,[a] Mingyang Chen,*[g,b] Faming Gao,[e] and Huiyang Gou*[a]

[a.] Center for High Pressure Science and Technology Advanced Research, Beijing 100094, China.

[b.] Beijing Computational Science Research Center, Beijing 100193, China.

[c.] Beijing Synchrotron Radiation Facility, Institute of High Energy Physics, Chinese Academy of Sciences, Beijing 100049, China.

[d.] Institute of Catalysis, Department of Chemistry, Zhejiang University, Hangzhou 310028, China.

[e.] College of Environment and Chemical Engineering, Yanshan University, Qinhuangdao, 066004, China.

[f.] Canada Canadian Light Source Saskatoon, Saskatchewan S7N2V3, Canada.

[g.] Center for Green Innovation, School of Materials Science and Engineering, University of Science and Technology Beijing, Beijing 100193, China.

[1] W. F. P., J. K. L., and K.Q.S. are contributed equally.

Email: huiyang.gou@hpstar.ac.cn.

Email: mychen@ustb.edu.cn.

Experimental Section

1. Synthesis of iron nickel monophosphosulfide.

Nickel powder (purity, > 99.99%; diameter, ~60 nm), iron powder (purity, > 99.99%; diameter, ~60 nm) and red phosphorus (purity, > 99.999%; diameter, 1~5 mm) are purchased from Aladdin Chemical Co., Ltd. Potassium hydroxide (KOH, AR; density, 2.130 g·cm^{-2}) and Nafion is purchased from Tianjin Komiou Chemical Reagent Co., Ltd. All the materials are used without any further purification in this experiment. $Ni_{1-x}Fe_xPS$ is synthesized by the high temperature and high pressure (HTHP) technique in a cubic multi-anvil system (CS−1B type, Guilin, China). The assemblies contain pyrophyllite pressure medium, graphite heater and *h*-BN capsule. Temperature is calibrated using W-Re (type C) thermocouples. Typical synthetic steps are as follows: firstly, stoichiometric Ni, P, S and Fe powders (Ni: Fe: P: S=1-*x*: *x*: 1: 1, *x* =0, 0.1, 0.15, 0.2) for $Ni_{1-x}Fe_xPS$ are mixed in a glove box (Ar atmosphere, O_2&H_2O < 0.1 ppm). Subsequently, the mixtures are pre-pressed into a cylindrical block precursor (Ø 5 mm × 3 mm) at ~ 20 MPa, and encapsulated into *h*-BN capsules. Finally, the samples are treated at 1500 °C for 10 min under 5.0 GPa then quenched by switching off the power. The ultrafine powder was obtained through high-energy mechanical milling (HEMM) method. All the samples are ball-milled using a planetary-type high energy ball milling with the ball to power ratio of 20:1 at 350 rpm for 10h under Ar atmosphere.

2. Morphology and structure analysis

X-ray diffraction (XRD) patterns are collected using a PANalytical X'Pert Pro X-ray diffractometer with Cu Kα radiation (λ = 0.15406 nm) at a scan rate of 0.013° min^{-1}. The morphology is characterized by field emission scanning electron microscopy (FESEM, JSM-7900F) and transmission electron microscopy (TEM&HRTEM, JEOL2010, Japan) equipped with X-ray energy-dispersive spectroscopy detector (EDS). And the high-resolution TEM (HRTEM) and element mapping were performed at 200 kV. The chemical states of the elements are characterized by X-ray photoelectron spectroscopy (XPS, AXIS Ultra DLD, Japan) with a monochromatic Al Kα X-ray source. Raman spectra are obtained using a confocal micro-Raman

spectroscopy (LabRam HR Evolution, Horiba) equipped with a 488 nm excitation laser and an 1800 lines/mm grating monochromator. The XAS data were collected at Beamline 1W1B at the Beijing Synchrotron Radiation Facility (BSRF). The storage ring is operated at 250 mA mode with a Si (111) double crystal monochromator to produce Monochromatic X-rays. The energy calibrations of the monochromator are checked by K-edge of Fe foil (7112 eV) and Ni foil (8333 eV), respectively. XAS spectra of Ni (Fe) K-edge in $Ni_{1-x}Fe_xPS$ are collected in transmission (fluorescence) mode and all of the reference samples are performed in transmission mode. All XAS data fitting are processed using the ATHENA program of IFEFFIT software packages and analyzed in the WINXAS software. The scattering pathways from NiS_2 (for NiPS before OER) and FeS_2 (for $Ni_{0.85}Fe_{0.15}PS$ before OER) crystal structures were used as the theoretical fitting model for before OER. A modified scattering pathway from NiPS-NiOOH (for NiPS after OER) and FeS_2-FeOOH (for $Ni_{0.85}Fe_{0.15}PS$ after OER) crystal structures were used as the theoretical fitting model for after OER.

3. Electrode preparation.

All electrodes are prepared by drop-casting the obtained catalyst suspension on the pre-cut nickel foams (thickness: 1.5 mm, geometric effective dimensioning:1x1 cm) and the loading mass is 4.0 mg. The catalyst ink is prepared by mixing 1ml water/ethanol (Volume ratio is 1:3), 50 ul Nafion (Nafion D-521 dispersion, 5% w/w in water and 1-propanol, ≥0.92 meq/g exchange capacity) and 4 mg $Ni_{1-x}Fe_xPS$, reference RuO_2 catalysts, then ultrasound treating over 30 min. Finally, these nickel foams with catalyst are dried in air over 5 h.

4. Electrochemical measurements.

All electrochemical measurements are performed on an electrochemical workstation (Model CHI770E), using a typical three-electrode electrochemical system. Hg/HgO (1 M KOH) electrode as the reference electrode and a Platinum electrode(1cm×1cm) as the counter electrode, the sample coated nickel foam electrodes (1cm×1cm) are evaluated as the working electrode. All potentials of this study are based on reference reversible hydrogen electrode (RHE): E(RHE)= E(Hg/HgO)+0.098V+0.0591×pH, and the overpotential (η) is calculated according to the formula: η= E(RHE) -1.23 V. All the electrochemical tests are performed in O_2-saturated 1.0 M KOH solution at room temperature. Linear sweep voltammetry (LSV) is collected at a scan rate of 5 mV s^{-1}. Tafel slopes are obtained from the linear part of Tafel curve obtained by reference formula: η = b*log(j)+a. The electrochemically active surface areas are estimated by calculating the current contribution of the electrochemical double-layer capacitance in total current. Cyclic voltammograms (CV) cures are recorded in the region of 0.05 – 0.1 V (vs. RHE) with various scan rates (v=20, 40, 60, 80 and 100 mV s^{-1}). Electrochemical impedance spectroscopy (EIS) is collected at 0.45 V (vs. SCE) in a frequency range from 100k Hz to 0.01 Hz. Chronoamperometric test is conducted at the constant current density of about 50 $mA \cdot cm^{-2}$. The materials (deposited on carbon cloth) are measured in CV model at rate of 100mV/s from 1.23V vs. RHE to potential where current density is 100mA/cm^2, after two hours' reaction, the samples are collected defined as after OER.

5. Computational Details.

The OER performance of NiPS and Fe-regulated NiPS models were evaluated using first-principles density functional theory (DFT).[1] Bulk NiPS (Pa-3)[2] was first optimized using a unit cell with both lattice parameters and ion positions fully relaxed. The optimized lattice parameter is

a =5.551 Å, which agrees well with the experimental values of a= 5.551 Å (Table S1). NiPS (102) slab is constructed with a 2×1×2 supercell of the (102) cleaved surface and it contains 4 layers with 14 Ni, 16 P and 16 S atoms. A 15 Å vacuum was placed to separate the slab and its images. Fe-regulated NiPS (102) slab was generated by substituting a Fe for a surface Ni of NiPS (102) supercell. Gibbs free energy profiles for the oxygen evolution reactions were predicted for the surface Ni of NiPS (102) and for the surface Fe of Fe-doped NiPS (102). The 4-electrons mechanism[3] by Norskov was considered for the OER activities of NiPS and Fe-regulated NIPS, in the following five steps:

$$OH^- + * \rightarrow *OH + e^- \quad (1)$$

$$*OH \rightarrow *O + H^+ + e^- \quad (2)$$

$$OH^- + *O \rightarrow *OOH + e^- \quad (3)$$

$$*OOH \rightarrow *O_2 + H^+ + e^- \quad (4)$$

$$*O_2 \rightarrow * + O_2 \quad (5)$$

where the * denotes a site on the surface (* by itself denotes a free site and *O denotes an oxygen atom adsorbed on the surface), while OH, O, OO, and OOH are surface adsorbates in the OER intermediate species. Among steps (1) to (5), the first four steps are electron-transfer steps that are key to the electrochemical catalysis. The Gibbs free energy (G) of the OER species is evaluated by correcting the calculated electronic energy with the zero-point energy correction (ZPE) and the entropy correction (TS). ZPEs and entropy corrections were obtained either based on the vibrational frequency calculations (for slabs) or from available thermodynamics database (for gas-phase molecules).[4] The overall OER has a free energy change of 4.92 eV, because of the reduction potential difference of the water-splitting half reactions (i.e. 1.23 eV for each electron transfer step).[5]

The reaction free energy change (ΔG), also referred as reaction energy barrier, for the elementary OER steps (equation 1-5) with respect to the standard hydrogen electrode (SHE) can be calculated as following equations:

$$\Delta G_1 = G(*OH) - G(H_2O) + \frac{1}{2}G(H_2) - G(*) \quad (6)$$

$$\Delta G_2 = G(*O) + \frac{1}{2}G(H_2) - G(*OH) \quad (7)$$

$$\Delta G_3 = G(*OOH) - G(H_2O) + \frac{1}{2}G(H_2) - G(*O) \quad (8)$$

$$\Delta G_4 = G(*O_2) + \frac{1}{2}G(H_2) - G(*OOH) \quad (9)$$

$$\Delta G_5 = 4.92 - (\Delta G_1 + \Delta G_2 + \Delta G_3 + \Delta G_4) \quad (10)$$

All of DFT-level geometry optimization calculations, electronic structure calculations, and vibrational frequency calculations are performed using Vienna ab initio simulation package (VASP)[6]. The DFT calculations are carried out with the Perdew-Burke-Ernzerhof (PBE) exchange-correlation functional[7] and the projected augmented wave (PAW)[8,9] potentials. The electronic wave functions are expanded using plane wave with energy cutoff of 600 eV. The Brillouin zone is sampled using a 4×4×4 Monkhorst-Pack grid[10] for the calculations of the bulk structure and a 4×4×1 Monkhorst-Pack grid for the calculations of the slabs (for OER

calculations). The convergence criteria for the energy and force during the geometry optimization calculations are set to 10^{-5} and 0.01 eV/Å.

Table S1: Crystal-structural parameters of the NiPS and $Ni_{0.85}Fe_{0.15}PS$ from Rietveld refinement.

Composition		**NiPS**	**$Ni_{0.85}Fe_{0.15}PS$**
Space group		$Pa\bar{3}$ (205)	$Pa\bar{3}$ (205)
Phase structure		Cubic	Cubic
a=b=c (Å)		5.551	5.529
V ($Å^3$)		171.046	169.021
Z		4	4
Atom site	Ni	(0.000, 0.000, 0.000)	(0.000, 0.000, 0.000)
	Fe	--	(0.000, 0.000, 0.000)
	P	(0.388, 0.388, 0.388)	(0.388, 0.388, 0.388)
	S	(0.388, 0.388, 0.388)	(0.388, 0.388, 0.388)

Table S2: Comparison of OER electrocatalysts in 1M KOH for similar reported systems.

Catalyst	j (mA cm^{-2})	η (mV)	Tafel (mV dec^{-1})	Electrolytes	Ref.
$Ni_{0.85}Fe_{0.15}PS$	10 100	251 314	34	1.0 m KOH	This work
FeS_2/CoS_2 NS	100	302	44	1.0 m KOH	11
Pt-CoS2/CC	10	300	58	1.0 m KOH	12
O-CoMoS	10	272	45	1.0 m KOH	13
NiS_2	10	264	105	1.0 m KOH	14
CoPS	10	308.1	58	1.0 m KOH	15
$Ni_{0.9}Fe_{0.1}PS_3$	20	329	69	1.0 m KOH	16
V- NiS_2 NS	10	290	45	1.0 m KOH	17
$NiS_2/CoS_2/C$	20	310	78	1.0 m KOH	18
$NiPS_3$@G-1:1	10	294	42.6	1.0 m KOH	19
LSTL $NiPS_3$	10	300	88	1.0 m KOH	20
S:CoP NPs	10	300	82	1.0 m KOH	21
$CeO_2/CoSe_2$	10	290	44	1.0 m KOH	22
$NiP_{0.62}S_{0.38}$	10 100	240 380	--	1.0 m KOH	23
$Fe_{0.09}Co_{0.13}$-$NiSe_2$/CFC	10	251	63	1.0 m KOH	24
Zn-doped $CoSe_2$/CFC	10	356	88	1.0 m KOH	25

Table S3: TOFs values of $Ni_{1-x}Fe_xPS$.

	NiPS	**$Ni_{0.9}Fe_{0.1}PS$**	**$Ni_{0.85}Fe_{0.15}PS$**	**$Ni_{0.8}Fe_{0.2}PS$**
$TOF_{\eta=450\ mV}$ (10^{-3} S^{-1})	21	47	97	75
$TOF_{\eta=400\ mV}$ (10^{-3} S^{-1})	8	22	58	42
$TOF_{\eta=350\ mV}$ (10^{-3} S^{-1})	3	8	25	19
$TOF_{\eta=300\ mV}$ (10^{-3} S^{-1})	0.4	2	7	5

Table S4: The fitting results of EIS spectra.

	NiPS	**$Ni_{0.9}Fe_{0.1}PS$**	**$Ni_{0.85}Fe_{0.15}PS$**	**$Ni_{0.8}Fe_{0.2}PS$**
Rs(Ω)	1.728	1.713	1.712	1.712
Rc(Ω)	15.990	3.853	1.857	2.430

Table S5: Chemical compositions detected by the energy dispersive X-ray (EDX) elemental mapping

Samples	Elenmets	Weight (wt%)	Atom (at%)
NiPS	Ni K	47.2	32.4
	P K	26.2	34.1
	S k	26.6	33.5
$Ni_{0.9}Fe_{0.1}PS$	Ni K	41.4	28.2
	Fe K	4.2	3.0
	P K	28.1	36.2
	S K	26.3	32.7
$Ni_{0.85}Fe_{0.15}PS$	Ni K	41.1	28.2
	Fe K	6.6	4.8
	P K	26.0	33.9
	S K	26.3	33.1
$Ni_{0.8}Fe_{0.2}PS$	Ni K	36.3	24.7
	Fe K	1.1	7.0
	P K	27.5	35.5
	S K	26.4	32.9

Table S6: Fitting parameters in the first shell of Ni and Fe K-edge EXAFS curves for NiPS, $Ni_{0.85}Fe_{0.15}PS$ before and after OER.

Sample	path	CN[a]	$\sigma^2(10^{-3}Å^2)$[b]	ΔEo (eV)[c]	R (Å)[d]
NiPS	Ni – S (P)	6.0	7.9	-4.25	2.30
$Ni_{0.85}Fe_{0.15}PS$	Ni – S (P)	6.0	7.9	-4.33	2.29
NiPS after OER	Ni-O	7.2	7.5	2.01	2.04
	Ni – S (P)	5.5	5.0		2.39
$Ni_{0.85}Fe_{0.15}PS$ after OER	Ni-O	6.3	8.8	5.08	2.02
	Ni – S (P)	4.6	6.7		2.41
$Ni_{0.85}Fe_{0.15}PS$	Fe – S (P)	6	5.5	1.57	2.25
$Ni_{0.85}Fe_{0.15}PS$ after OER	Fe-O	5.6	5.1	5.76	2.07
	Fe – S (P)	5.4	5.00		2.20

[a] the average coordination number CN (CN was set as theoretical value during fitting before OER). [b] Debye-Waller factor σ^2 was set in a range of 0.005 to 0.01. [c] inner potential shift ΔEo was set to equal and in a range of -6 to 6 eV. [d] R is the interatomic distance from the central scattering atom.

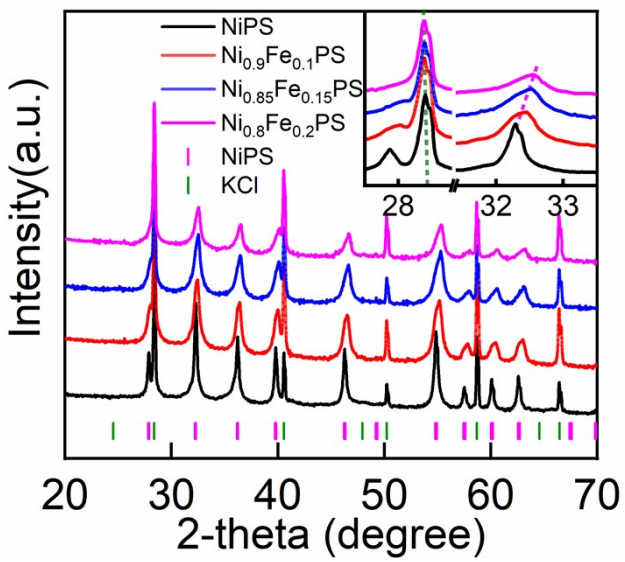

Figure S1: XRD patterns of $Ni_{1-x}Fe_xPS$ (x = 0, 0.1, 0.15, 0.2) using KCl as the internal standard for the correction of the diffraction angle.

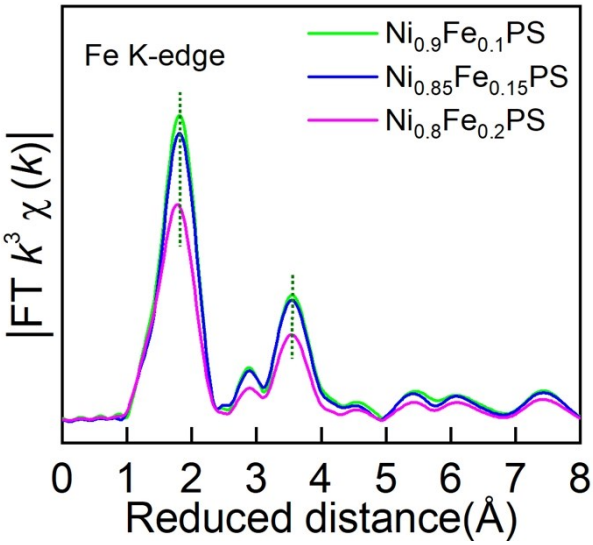

Figure S2: FT curves of Fe K-edge EXAFS $k^3\chi(k)$ of $Ni_{1-x}Fe_xPS$.

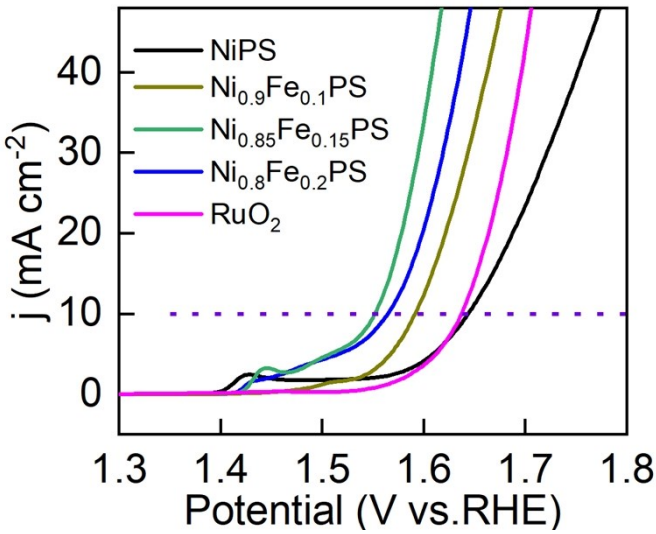

Figure S3: LSV curves of $Ni_{1-x}Fe_xPS$ and RuO_2 measured on glassy carbon (GC).

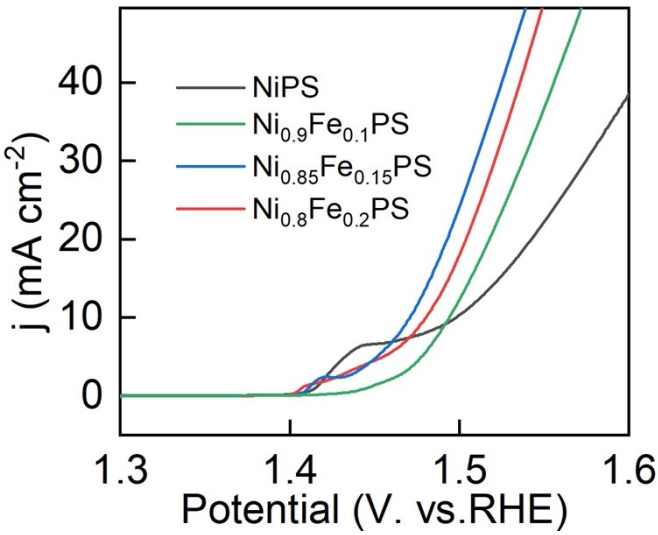

Figure S4: LSV curves without ir-correction of $Ni_{1-x}Fe_xPS$ on Ni foam.

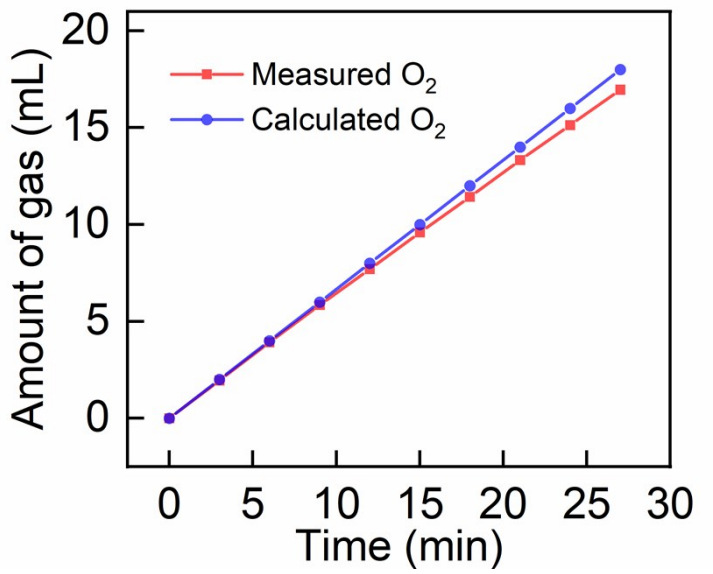

Figure S5: The electrocatalytic efficiency of $Ni_{0.85}Fe_{0.15}PS$ for OER.

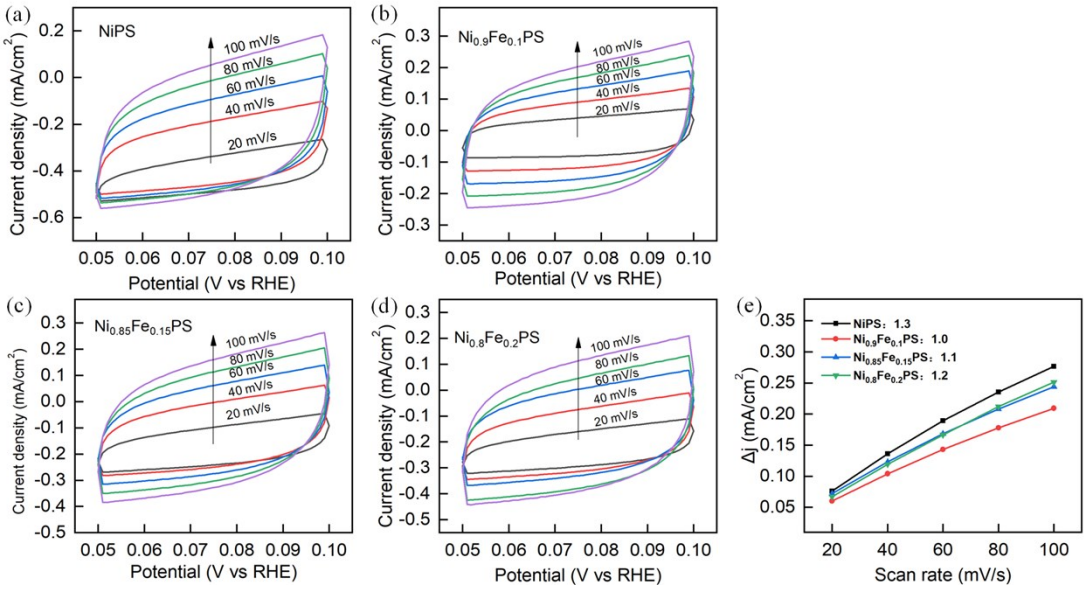

Figure S6: (a-d) Electrochemical cyclic voltammogram of $Ni_{1-x}Fe_xPS$ at various potential scanning rates and (e) the extraction of C_{dl}.

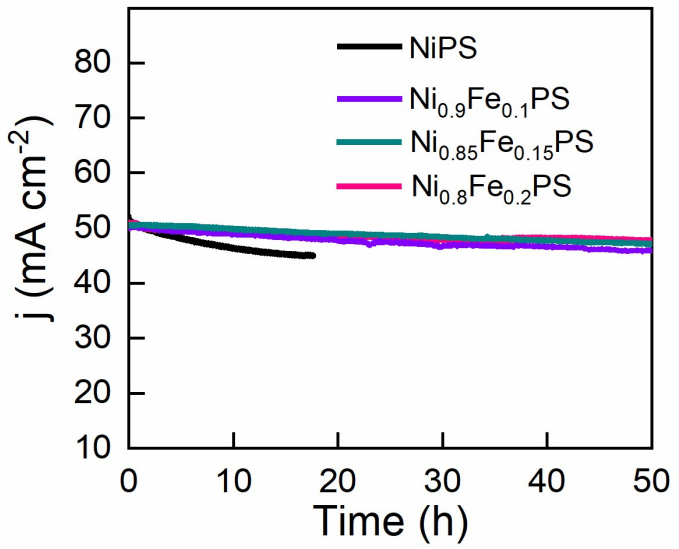

Figure S7: The chronoamperometric curve of $Ni_{1-x}Fe_xPS$ (x=0, 0.1, 0.15 and 0.2) (on Ni foam) in 1.0 M KOH. The initial current density was about 50 mA cm^{-2}.

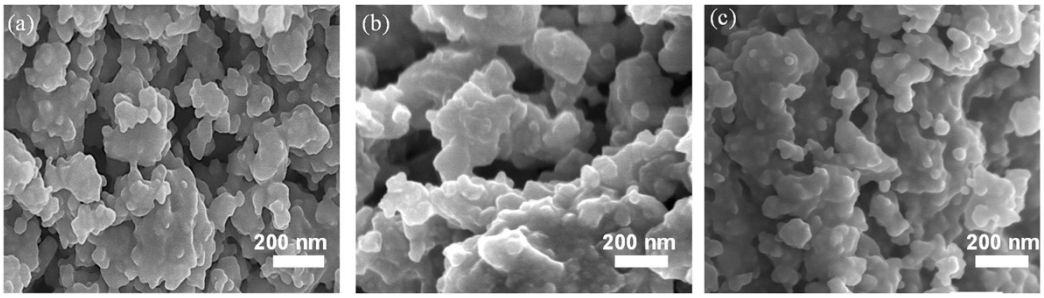

Figure S8: SEM images of NiPS (a), $Ni_{0.9}Fe_{0.1}PS$ (b), $Ni_{0.8}Fe_{0.2}PS$ (c) before OER.

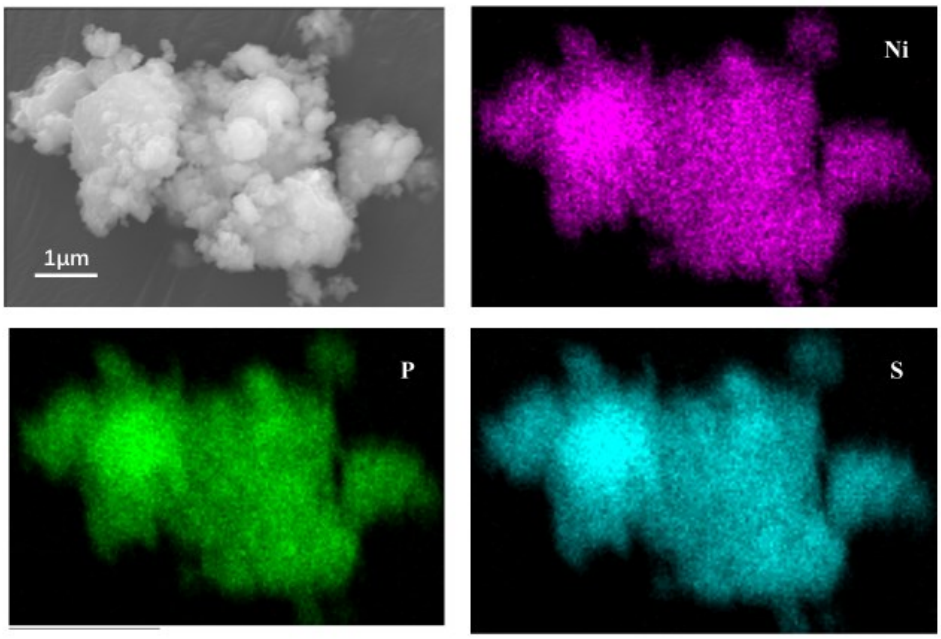

Figure S9: SEM-EDX elemental mapping of NiPS before OER.

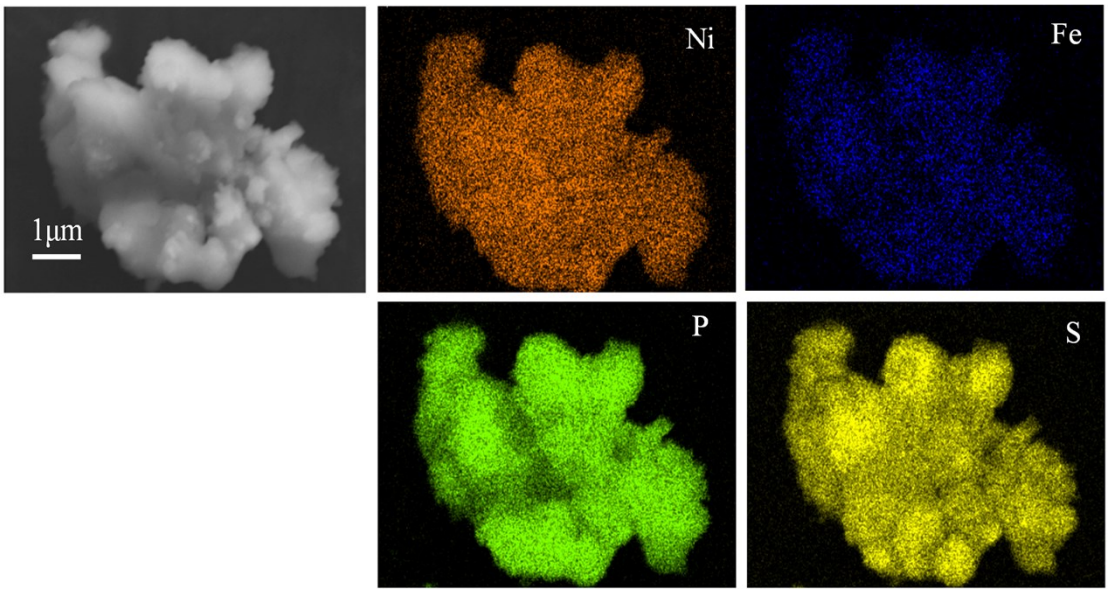

Figure S10: SEM-EDX elemental mapping of $Ni_{0.9}Fe_{0.1}PS$ before OER.

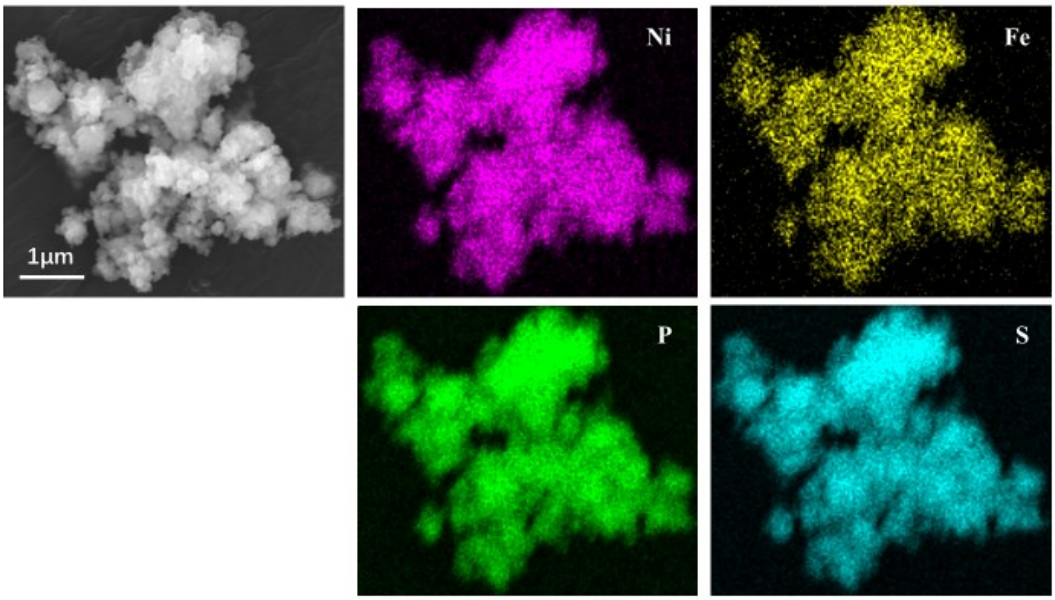

Figure S11: SEM-EDX elemental mapping of $Ni_{0.85}Fe_{0.15}PS$ before OER.

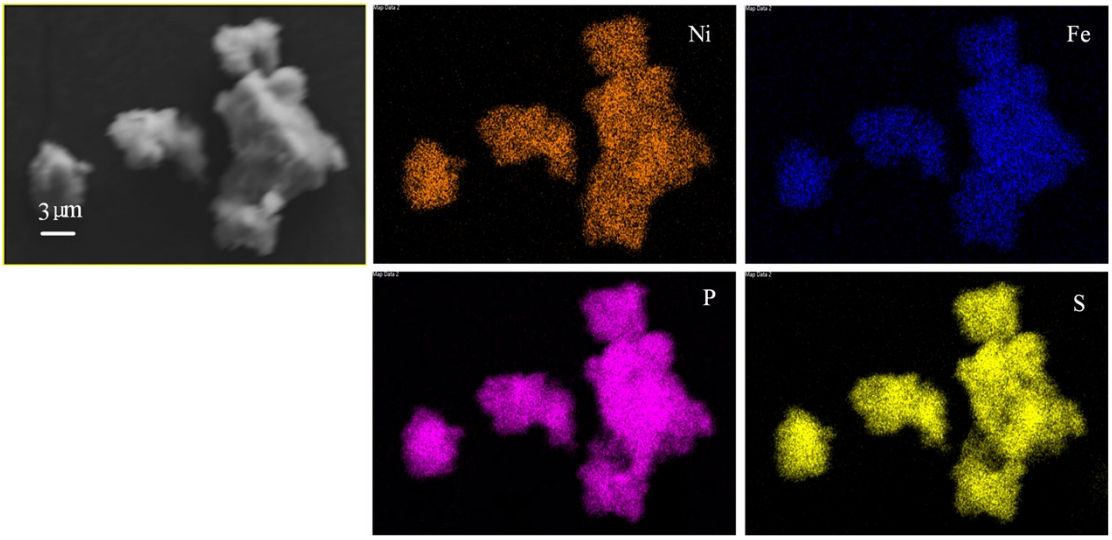

Figure S12: SEM-EDX elemental mapping of $Ni_{0.8}Fe_{0.2}PS$ before OER.

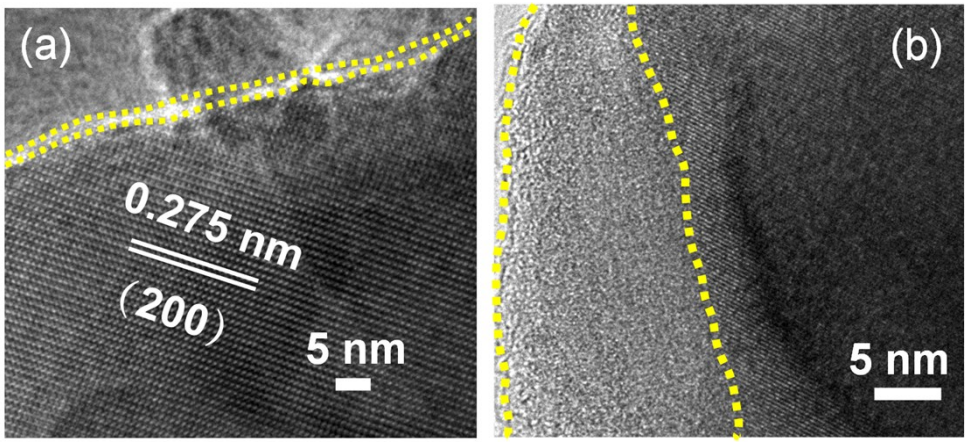

Figure S13: HRTEM images of the $Ni_{0.85}Fe_{0.15}PS$ (a) before and (b) after electrocatalysis.

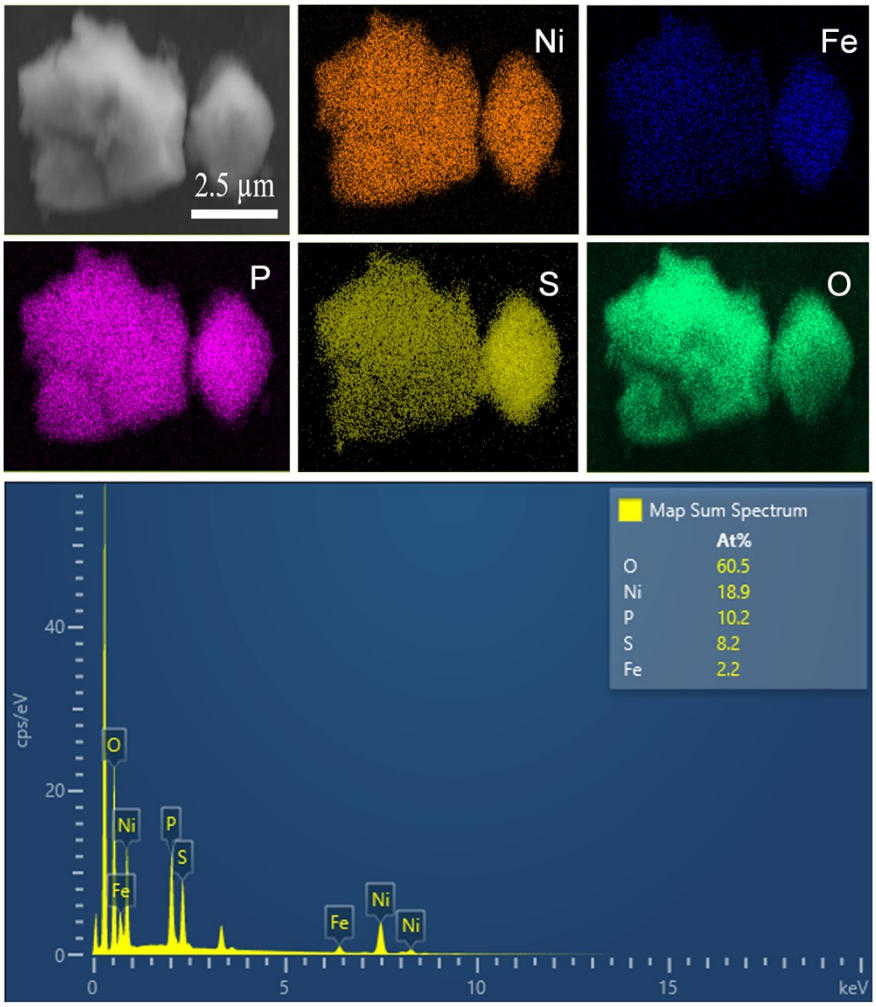

Figure S14: Collected XRD patterns of $Ni_{0.9}Fe_{0.1}PS$ before and after OER.

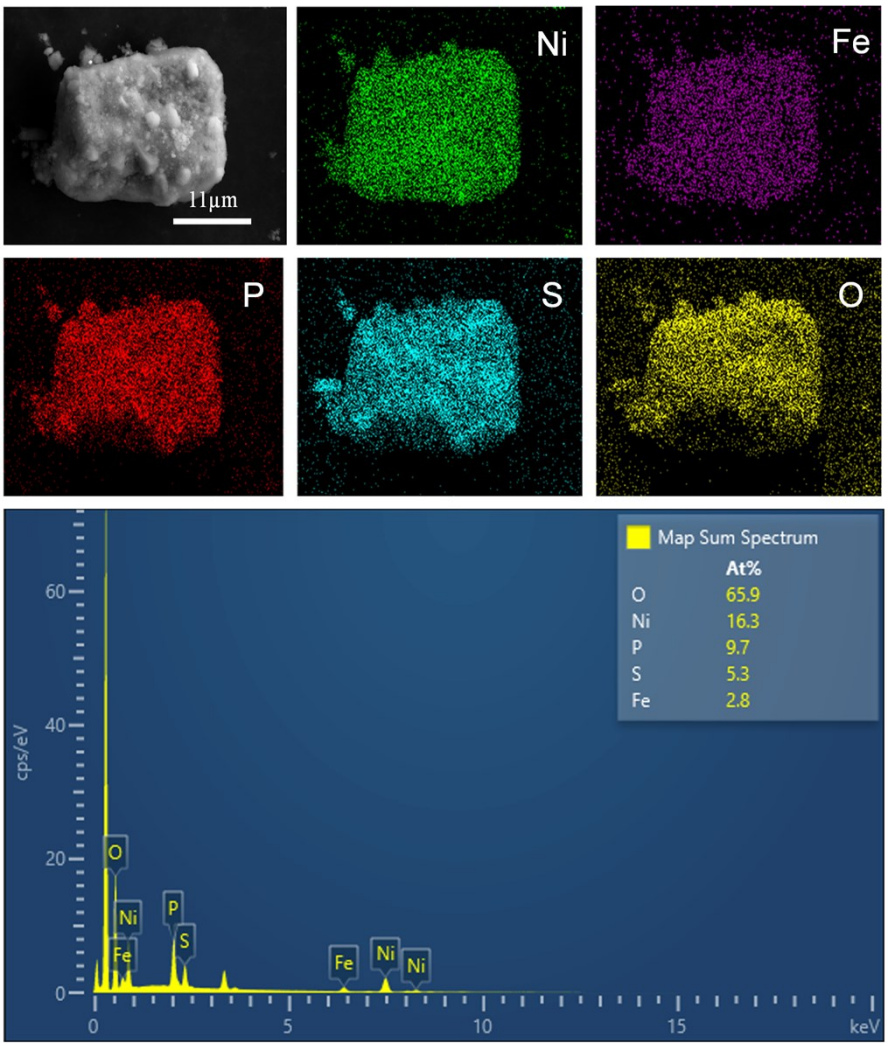

Figure S15: Collected XRD patterns of $Ni_{0.85}Fe_{0.15}PS$ before and after OER.

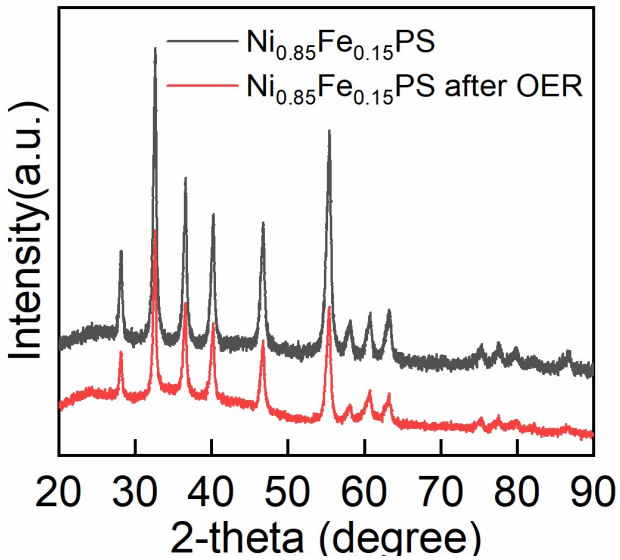

Figure S16: Collected XRD patterns of $Ni_{0.85}Fe_{0.15}PS$ before and after OER.

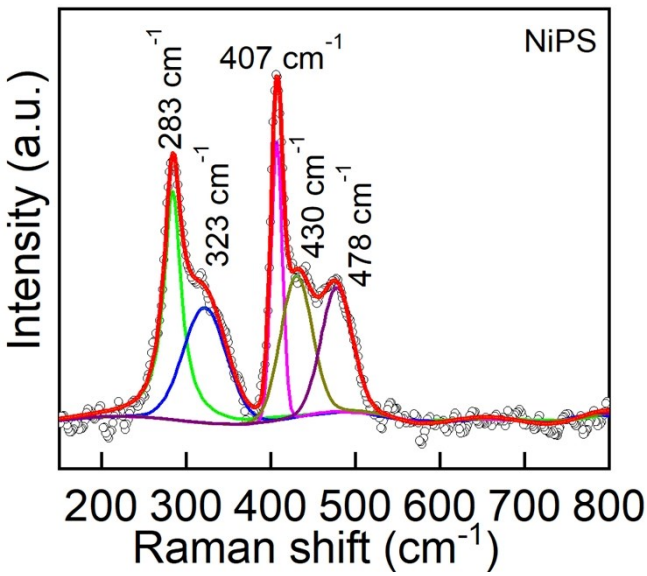

Figure S17: Raman spectra of NiPS before OER.

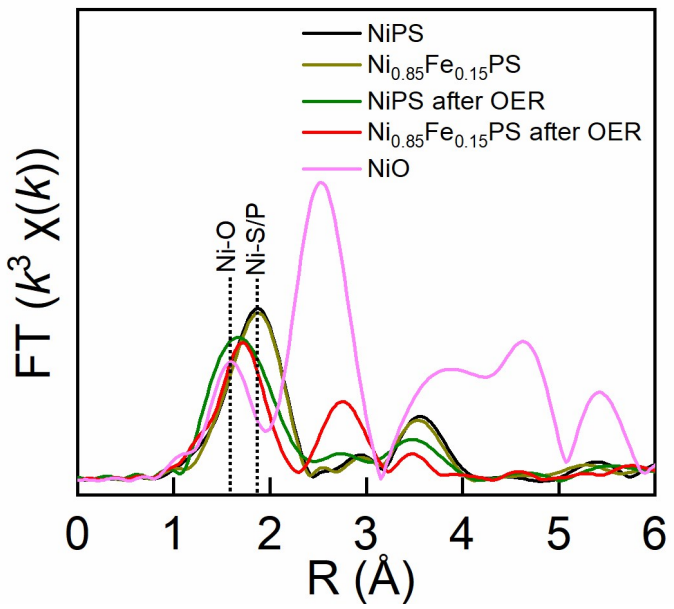

Figure S18: FT of EXAFS k^3 $\chi(k)$ spectra of NiPS and $Ni_{0.85}Fe_{0.15}PS$ before and after OER with NiO as references.

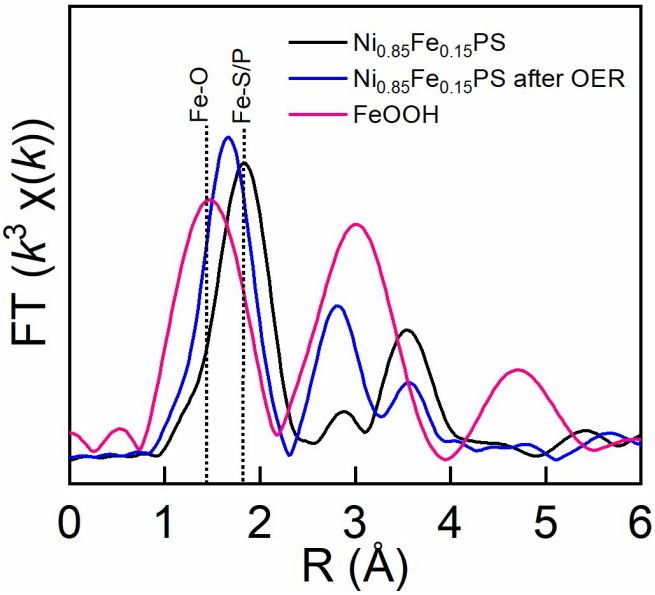

Figure S19: FT of EXAFS k^3 $\chi(k)$ spectra of $Ni_{0.85}Fe_{0.15}PS$ before and after OER with FeOOH as references.

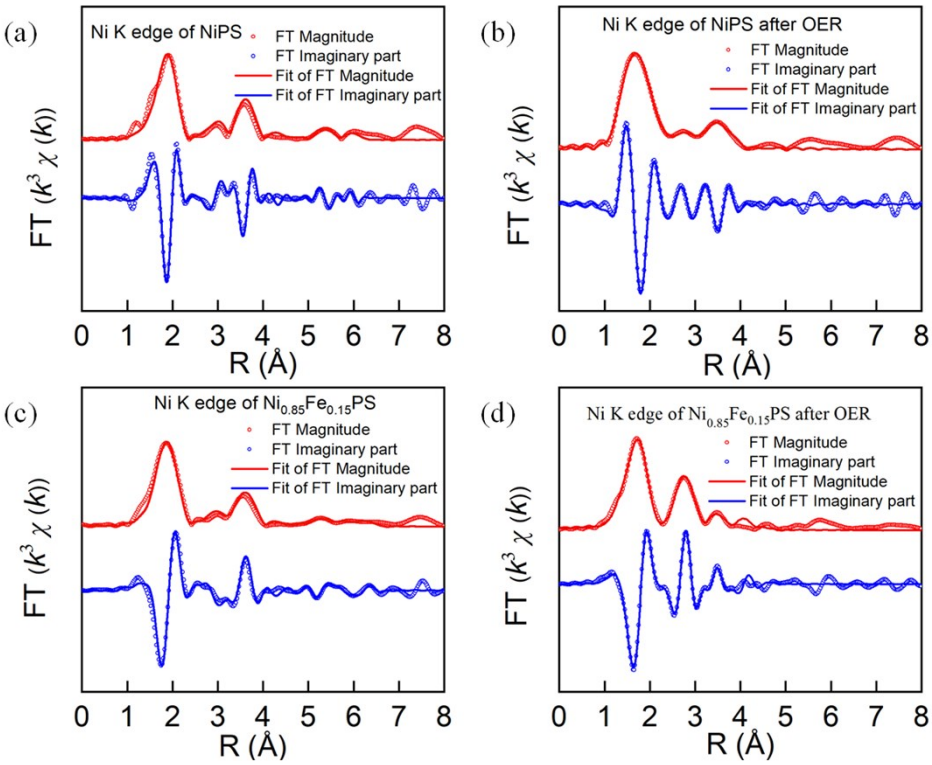

Figure S20: Fourier transformed k^3 weight EXAFS oscillations measured at Ni K-edge and corresponding fitting results of NiPS and $Ni_{0.85}Fe_{0.15}PS$ before and after OER.

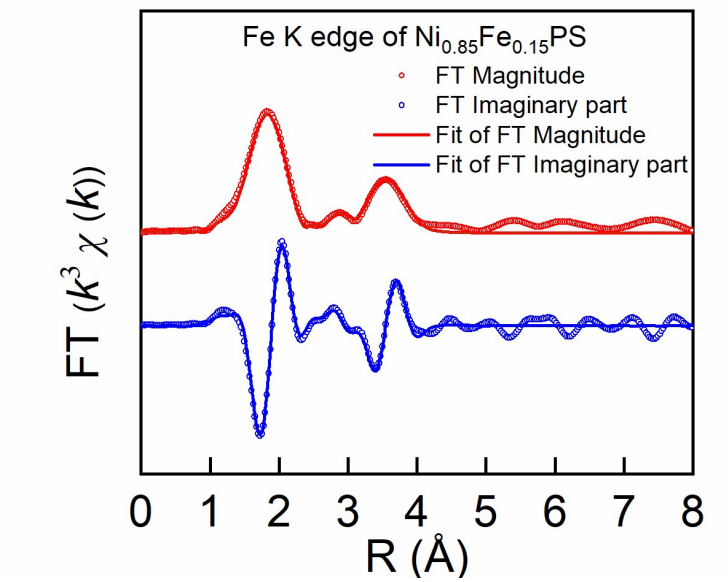

Figure S21: Fourier transformed k^3 weight EXAFS oscillations measured at Fe K-edge and corresponding fitting result of the $Ni_{0.85}Fe_{0.15}PS$ catalyst before OER.

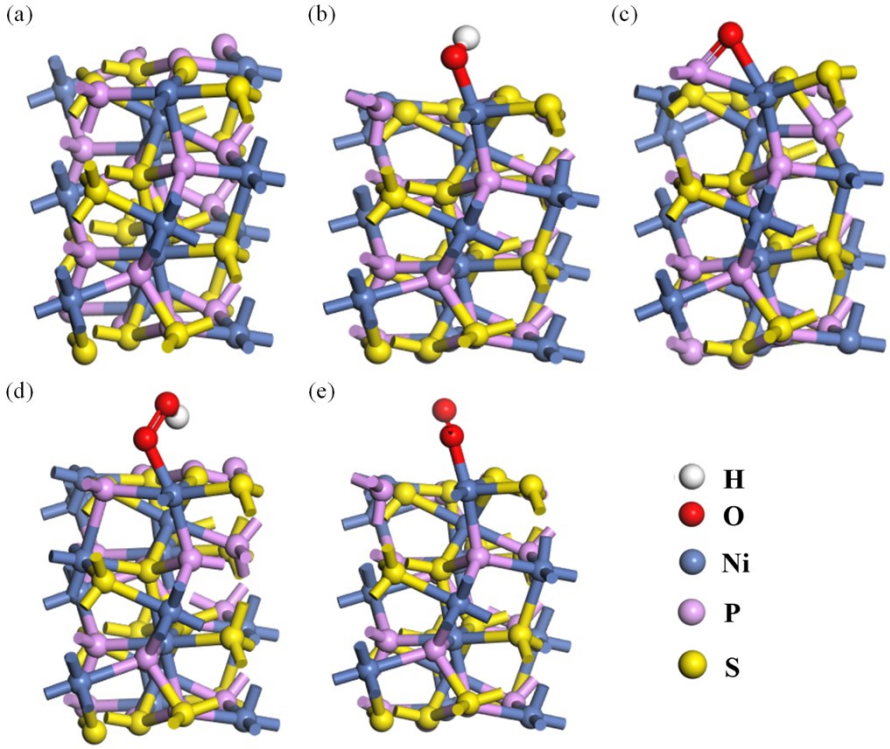

Figure S22: The optimized structures for the OER species at the surface Ni site of pure NiPS (102): (a) free site * (b) *OH (c) *O (d) *OOH and (e) *OO.

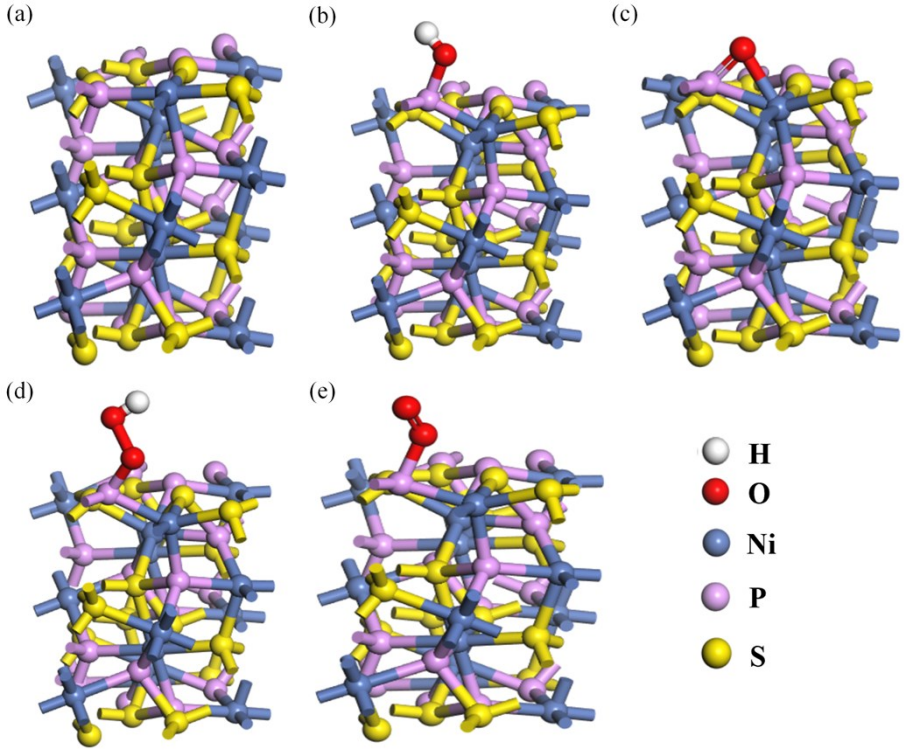

Figure S23: The optimized structures for the OER species at the surface P site of pure NiPS (102): (a) free site * (b) *OH (c) *O (d) *OOH and (e) *OO.

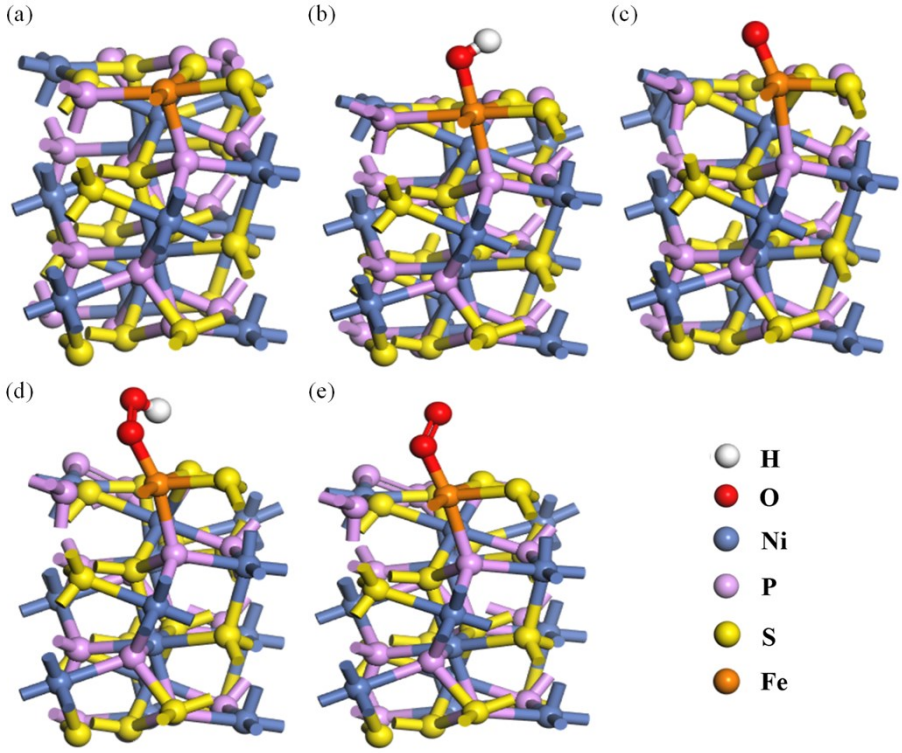

Figure S24: The optimized structures for the OER species at surface Fe site of Fe-doped NiPS (102): (a) free site * (b) *OH (c) *O (d) *OOH and (e) *OO.

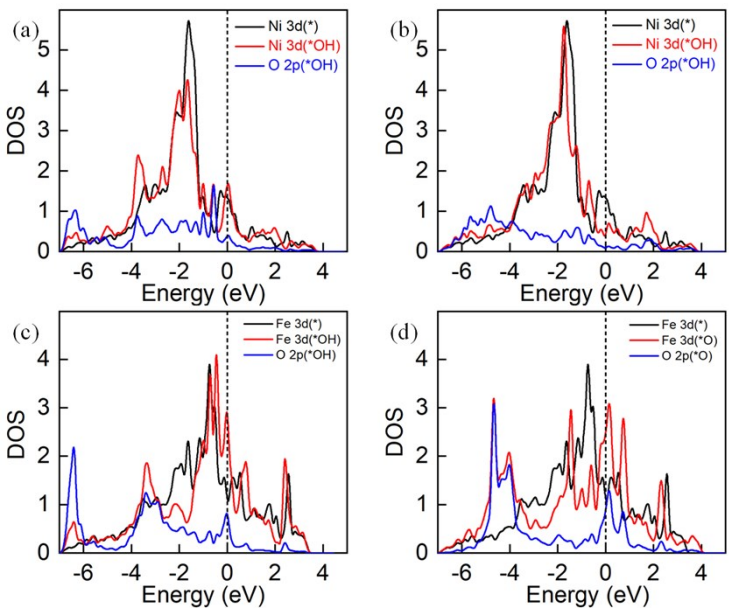

Figure S25: The surface Ni 3d and O 2p PDOS of (a)* and *OH, (b) * and *O. The surface Fe 3d and O 2p PDOS of (c) * and *OH, (d) * and *O.

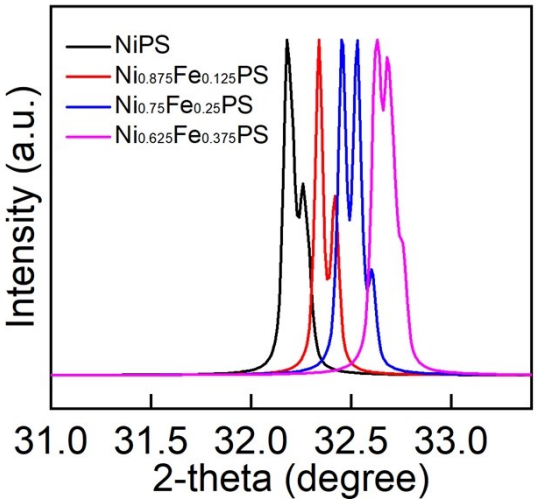

Figure S26: Predicted X-ray diffraction pattern for (200) of DFT-optimized NiPS, $Ni_{0.875}Fe_{0.125}PS$, $Ni_{0.75}Fe_{0.25}PS$ and $Ni_{0.625}Fe_{0.375}PS$.

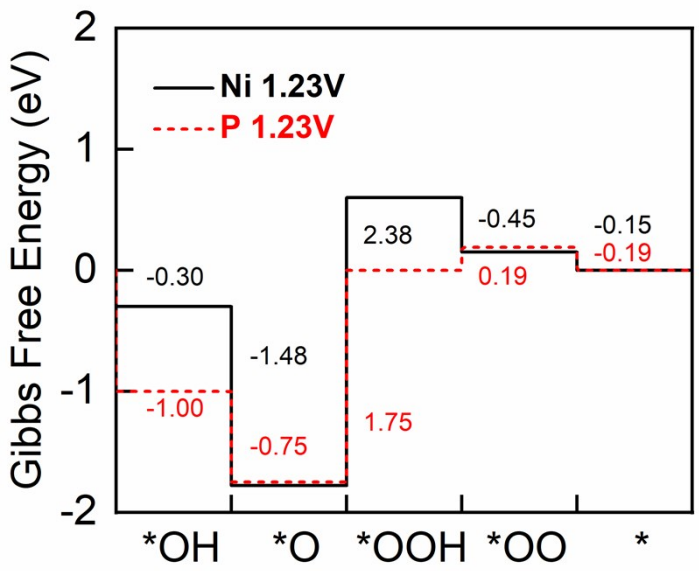

Figure S27: Calculated Gibbs free energy profiles for OER at the surface Ni and P sites on the (102) surface of NiPS at the external bias potential U = 1.23 V.

References for ESI

1 W. Kohn, L. J. Sham, *Phys. Rev. A*, 1985, **140**, 1133.

2 A. Jain, S. P. Ong, *APL Materials*, 2013, **1**, 011002.

3 J. K. Norskov, *J. Electrochem. Soc.*, 2005, **152**, J23.

4 X. G. Ma, B. Lu, D. Li, R. Shi, C. S. Pan, Y. F. Zhu, *J. Phys. Chem. C*, 2011, **115**, 4680.

5 R. Kishore, X. Cao, X. Zhang, A. Bieberle-Hütter, *Catalysis Today*, 2018, **94**, *321-322*.

6 G. Kresse, J. Furthmüller, *Phys. Rev. B*, 1996, **54**, 11169.

7 J. P. Perdew, K. Burke, M. Ernzerhof, *Phys. Rev. Lett.*, 1996, **77**, 3865.

8 G. Kresse, D. Joubert, *Phys. Rev. B*, 1999, **59**, 1758.

9 P. E. Blöchl, *Phys. Rev. B*, 1994, **50**, 17953.

10 H. J. Monkhorst, J. D. Pack, *Phys. Rev. B*, 1976, **13**, 5188.

11 Y. Li, J. Yin, L. An, M. Lu, K. Sun, Y. Q. Zhao, P. Xi, *Small*, 2018, **14**, 1801070.

12 X. Han, X. Wu, Y. Deng, J. Liu, J. Lu, C. Zhong, W. Hu, *Adv. Energy Mater.*,2018, **8**, 1870110.

13 J. Hou, B. Zhang, Z. Li, S. Cao, Y. Sun, Y. Wu, L. Sun, *ACS Catal*., 2018, **8**, 4612-4621.

14 P. Thangasamy, V. Maruthapandian, V. Saraswathy, M. Sathish, *Catal. Sci. Technol*., 2017, **7**, 3591-3597.

15 G. Hu, J. Xiang, J. Li, P. Liu, R. N. Ali, B. Xiang, *J. Catal*., 2019, **371**, 126-134.

16 B. Song, K. Li, Y. Yin, T. Wu, L. Dang, M. Cabán-Acevedo, J. R. Schmidt, *ACS Catal*., 2017, **7**, 8549-8557.

17 H. Liu, Q. He, H. Jiang, Y. Lin, Y. Zhang, M. Habib, L. Song, *ACS nano*, 2017, **11**, 11574-11583.

18 W. Xin, W. J. Jiang, Y. Lian, H. Li, S. Hong, S. Xu, J. S. Hu, *Chem. Commun*., 2019, **55**, 3781-3784.

19 S. Xue, L. Chen, Z. Liu, H. M. Cheng, W. Ren, *ACS nano*, 2018, **12**, 5297-5305.

20 X. Li, Y. Fang, J. Wang, B. Wei, K. Qi, H. Y. Hoh, Y. Zhang, *Small*, 2019, 1902427.

21 M. A. R. Anjum, M. S. Okyay, M. Kim, M. H. Lee, N. Park, J. S. Lee, *Nano energy*, 2018, **53**, 286-295.

22 M. R. Gao, Y. R. Zheng, J. Jiang, S. H. Yu, *Accounts chem. Res*., 2017, **50**, 2194-2204.

23 J. Luo, H. Wang, G. Su, Y. Tang, H. Liu, F. Tian, D. Li, *J. Mater. Chem. A*, 2017, **5**, 14865-14872.

24 Y. Sun, K. Xu, Z. Wei, H. Li, T. Zhang, X. Li, Y. Li, *Adv. Mater*., 2018, **30**, 1802121.

25 Q. Dong, Q. Wang, Z. Dai, H. Qiu, X. Dong, *ACS appl. Mater. Inter.*, 2016, **8**, 26902-26907.